

pubs.acs.org/NanoLett Letter

Tailoring Single- and Double-Sided Fluorination of Bilayer Graphene via Substrate Interactions

Jangyup Son, Huije Ryu, Junyoung Kwon, Siyuan Huang, Jaehyung Yu, Jingwei Xu, Kenji Watanabe, Takashi Taniguchi, Eunji Ji, Sol Lee, Yongjun Shin, Jong Hun Kim, Kwanpyo Kim, Arend M. van der Zande,* and Gwan-Hyoung Lee*



Cite This: Nano Lett. 2021, 21, 891-898



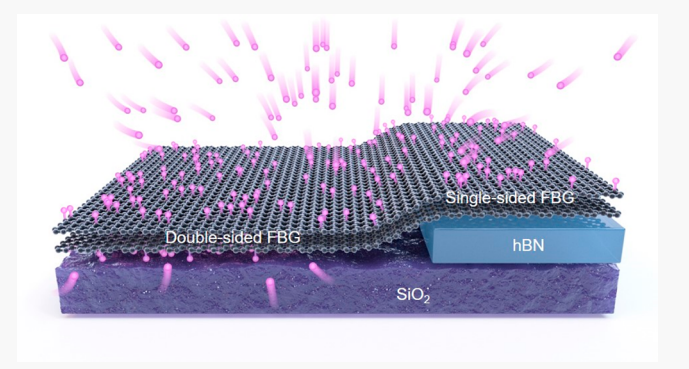
ACCESS I

Metrics & More



Supporting Information

ABSTRACT: While many technologies rely on multilayer heterostructures, most of the studies on chemical functionalization have been limited to monolayer graphene. In order to use functionalization in multilayer systems, we must first understand the interlayer interactions between functionalized and nonfunctionalized (intact) layers and how to selectively functionalize one layer at a time. Here, we demonstrate a method to fabricate single- or double-sided fluorinated bilayer graphene (FBG) by tailoring substrate interactions. Both the top and bottom surfaces of bilayer graphene on the rough silicon dioxide (SiO₂) are fluorinated; meanwhile, only the top surface of graphene on hexagonal boron nitride (hBN) is fluorinated. The functionalization type affects electronic properties; double-sided FBG on SiO₂



is insulating, whereas single-sided FBG on hBN maintains conducting, showing that the intact bottom layer becomes electrically decoupled from the fluorinated top insulating layer. Our results define a straightforward method to selectively functionalize the top and bottom surfaces of bilayer graphene.

KEYWORDS: Graphene, chemical functionalization, fluorination, substrate interaction, interlayer interactions

INTRODUCTION

An important emerging subclass of two-dimensional (2D) materials is "synthetic" 2D materials that have no bulk analogue. Since they are not accessible via mechanical exfoliation from bulk materials, new strategies are needed to produce these synthetic 2D materials. While some monoelemental synthetic 2D materials have been recently demonstrated through chemical vapor deposition, 1-3 in many cases, synthetic 2D materials are derived from monolayers of bulk materials modified using chemical functionalization, including examples like Janus transition metal dichalcogenides (TMDs) of MoSSe, 4 Janus graphene, and diamane. Since robust 2D monolayers are used as a framework, this strategy is straightforward and promising for the production of a new family of 2D materials with newly assigned functions, such as out-of-plane piezoelectricity, tunable friction and wettability,7 and metal-to-insulator transition.8 Graphene, widely used to study the fundamental physics in the 2D limit, 9-17 is a particularly promising template for functionalization because it is easy to restructure sp² bonds with other atoms to generate new synthetic graphene derivatives, such as graphene oxide, 18 hydrogenated graphene, 19 and fluorinated graphene. 20 The vast majority of studies on synthetic materials are on monolayers. However, in

many technologies, these synthetic materials must be integrated into 2D heterostructures and multilayers to form devices. In these cases, it is critical to understand how layers interact in functionalized multilayer systems, and how to tailor the interactions to achieve different stable states. For example, there have been reports on single-sided (functionalized surface of top layer and intact bottom layers) or double-sided functionalization (functionalized top and bottom surfaces) of bilayer graphene. 21-24 However, until now, there has been no demonstrated way to control between these different states (single- and double-sided functionalization of bilayer graphene), yet being able to tailor the structure is key to accessing different material states; double-sided functionalization of bilayer graphene can induce unprecedented chemical transformation into diamane, a diamond-like layered carbon structure, while single-sided functionalization of bilayer

Received: August 6, 2020 Revised: October 14, 2020 Published: October 20, 2020





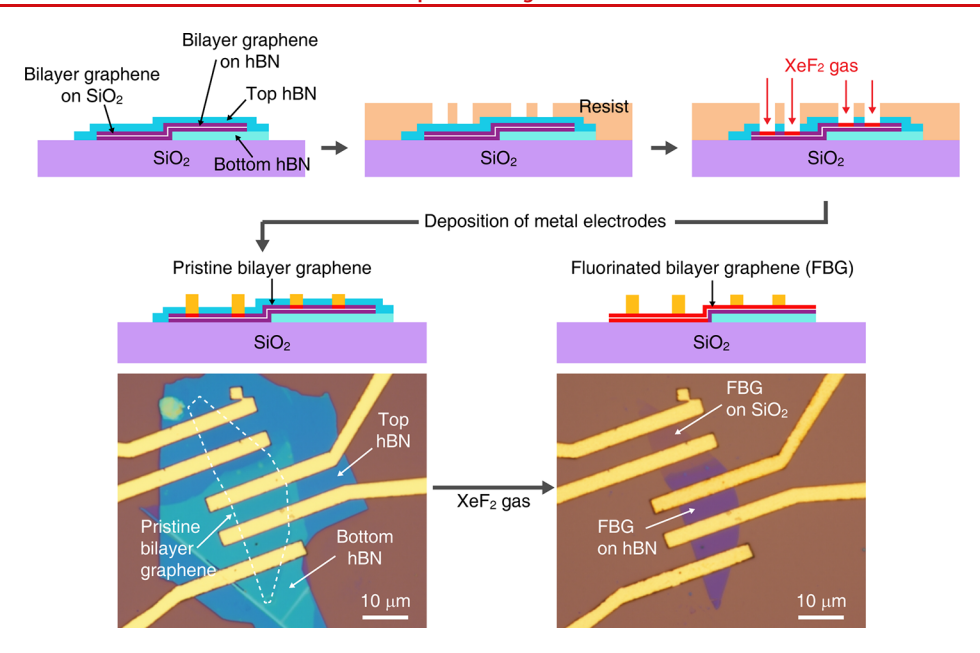


Figure 1. Schematic illustration of the fabrication process of the bilayer graphene device and the optical microscope images of the bilayer graphene device before and after exposure to XeF_2 gas. The patterning to make the electrical contact is performed by the electron beam lithography, and the exposed hBN is etched by XeF_2 gas; thus, embedded bilayer graphene is exposed. After deposition of metal electrodes, the bilayer graphene device is fabricated. All exposed hBN layers are etched first, and then, the embedded bilayer graphene is fluorinated while protecting the underlying bottom hBN.

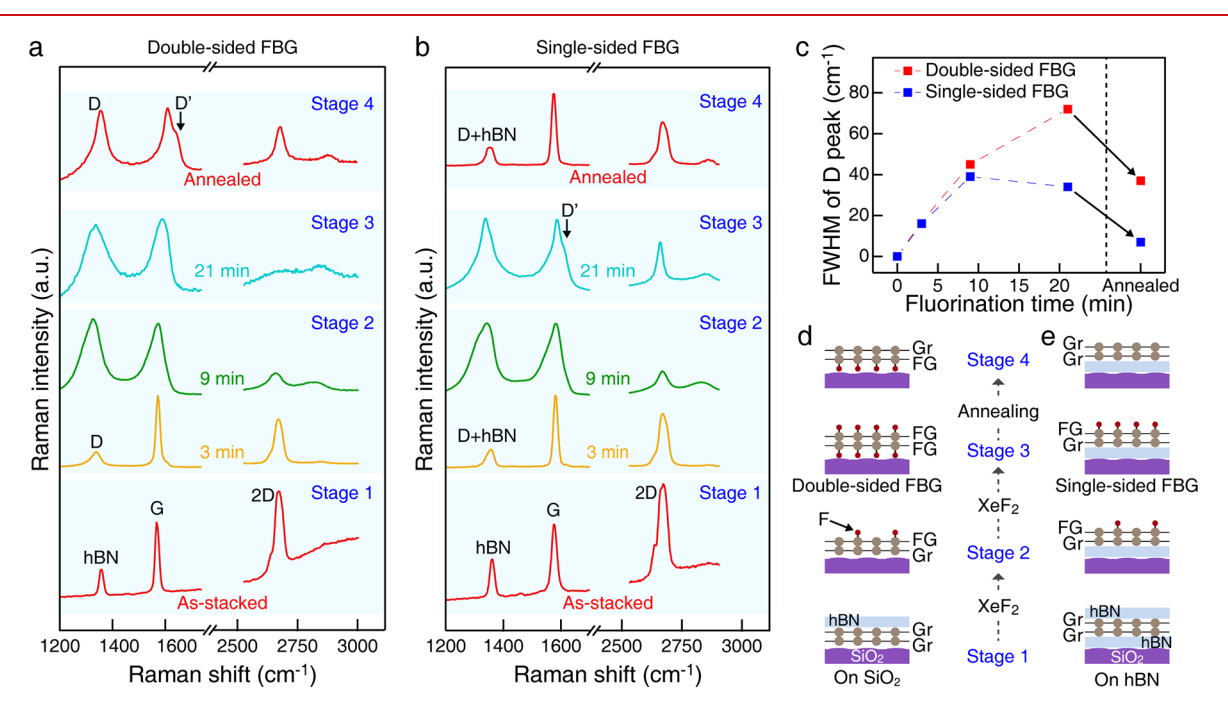


Figure 2. Difference in structural changes between bilayer graphene on SiO_2 and bilayer graphene on hBN via fluorination. Evolution in Raman spectra with an increase of fluorination time through four stages of (a) bilayer graphene on SiO_2 and (b) bilayer graphene on hBN. Stage 1, asstacked; Stage 2, after 3 min fluorination time; Stage 3, after 9 min fluorination time; Stage 4, after annealing. (c) Evolution of fwhm of D peaks for the bilayer graphene on SiO_2 and bilayer graphene on hBN via fluorination. Schematic illustration describing the evolution in fluorination of both (d) bilayer graphene on SiO_2 and (e) bilayer graphene on hBN. Bilayer graphene on SiO_2 is fluorinated to the form of double-sided FBG, and it is changed to single-sided FBG after annealing due to the defluorination of the top fluorinated graphene (FG) layer. Bilayer graphene on hBN is changed to single-sided FBG due to the absence of the penetration of XeF_2 gas into the graphene—hBN interface, and it is restored back to pristine bilayer graphene after annealing as the top FG is defluorinated.

graphene leads to a Janus material with both electrically conducting and insulating layers. 21,25

Here, we demonstrate a selective functionalization method for the fabrication of single- and double-sided fluorinated bilayer graphene (FBG) by tailoring the substrate interactions. Using Raman spectroscopy and electrical transport, we compare the evolution in fluorination structure and electronic properties of bilayer graphene exposed to xenon difluoride (XeF_2) gas on either rough silicon dioxide (SiO_2) or atomically smooth hexagonal boron nitride (hBN) substrates. We find

that the top surface of the upper layer of the bilayer graphene will always be fluorinated. However, selecting the supporting substrate between rough SiO2 and atomically smooth hBN enables the tuning of penetration of the gas through the interface with the bottom layer and the substrate and thus determines whether the bottom surface will also be fluorinated. From the evolution in the Raman spectra, we find that the bilayer graphene on SiO₂ exhibits double-sided fluorination, while the bilayer graphene on hBN exhibits only single-sided fluorination. The difference in structure is reflected in the electronic properties. The double-sided FBG on SiO₂ becomes insulating: meanwhile, the single-sided FBG on hBN stays conductive. This indicates that the bottom layer sandwiched by the fluorinated top layer and hBN in single-sided FBG is intact, maintaining intrinsic properties of monolayer graphene. 23,24 This study provides strategies for the fabrication of new 2D materials such as diamane,6 the preparation of structurally/ electrically decoupled 2D-layered materials, the innovative vertical patterning for engineering the physical, electronic, mechanical, and chemical properties of 2D functionalized materials, and the formation of C-F dipoles for spintronic and biomedical devices.

■ RESULTS AND DISCUSSION

Figure 1 shows the schematic illustrations for the fabrication of the bilayer graphene field-effect transistors (FETs) used in this study and optical microscopic images of the devices before and after exposure to XeF2 gas. We followed established methods for fabricating graphene heterostructure devices (see Figure S1 for additional transfer and fabrication details). 26,27 We first picked up an exfoliated bilayer graphene flake with a 10 nm hBN flake, and then transferred the stack onto a pre-exfoliated hBN flake. To directly compare the effect of the substrate on the chemical functionalization, the bilayer graphene was offset, so half the flake was placed on the hBN and the other half directly on the underlying SiO₂. The top hBN covers the whole stack and protects the underlying layers through the ensuing fabrication steps. To fabricate the devices, we leveraged a previously demonstrated capability where hBN is quickly etched when exposed to XeF2 gas, while graphene is only functionalized.²⁸ To access and electrically contact the buried graphene, we patterned electrodes, then etched through the exposed top hBN with XeF2 gas using the graphene etching stop (GES) technique, ²⁸ and finally deposited the metals into the etched regions (Figure S2). After the fabrication was completed, and initial measurements were performed, the devices were exposed to XeF2 gas again to etch away top hBN as shown in the final schematic of Figure 1. The top hBN was completely etched away, and bilayer graphene was fluorinated. However, the bottom hBN underneath the fluorinated graphene is protected from XeF2 due to the gas impermeability of graphene. 28,29 The fabricated FBG is very clean as the graphene was never directly exposed to any polymers or solvents during fabrication.²⁸

In Figure 2, we examine the substrate-dependent structure of FBG using Raman spectroscopy. Figure 2a,b shows the evolution in the Raman spectra of bilayer graphene on SiO_2 and hBN, respectively, during fluorination and annealing processes, through 4 distinct stages. The F-coverage on the graphene surface was successfully controlled with increasing fluorination time (Figure S3). In all stages, the Raman peak of hBN was observed at 1370 cm $^{-1}$. In Stage 1, the initial Raman spectra of the embedded bilayer graphene on hBN show a

broad 2D peak consisting of four single peaks right after stacking, which is an indicator of bilayer graphene (see Figure S4).30 There is also a broad background peak from 2500 to 3000 cm⁻¹, likely due to trapped residues as the background disappeared after fluorination and annealing.³¹ In Stage 2, during fluorination of 3-9 min, the D peak emerged and increased in intensity while the 2D peak decreased, indicating etching of top hBN and formation of C-F bonds in graphene on both SiO₂ and hBN.³²⁻³⁵ However, in Stage 3, the two substrates induce different fluorination behavior in the bilayer graphene. After fluorination for 21 min, the 2D peak of bilayer graphene on SiO2 was suppressed. This suppression has been observed in oxidized suspended bilayer graphene (doublesided oxidized bilayer graphene), 21 which is a sign that both surfaces of bilayer graphene are functionalized. In contrast, the 2D peak of bilayer graphene on hBN survived, close to that of monolayer graphene with high intensity and narrow width of a single Lorentzian (Figure S4). To understand this Raman spectrum, we compared it to a structure with two spatially decoupled graphene layers (see Figure S5). As shown in Figure S5, we fabricated a stack of fluorinated monolayer graphene and pristine monolayer graphene separated by thin hBN. The Raman spectrum of this stack after fluorination shows the combination of both narrow (from the bottom pristine graphene) and broad (from the top fluorinated graphene) peaks as we observed in Figure 2b (Stage 3). Although the 2D peak of single-sided FBG is broader than that of the sample shown in Figure S5b (see the fwhm plot in Figure S5c), from this comparison, we infer that the narrow 2D peak of singlesided FBG originates from a pristine bottom monolayer graphene covered by fluorinated top monolayer graphene, and the two layers have effectively decoupled, leading to the independent Raman response. In addition, the full width halfmaximum (fwhm) values of D peaks in both double- and single-sided FBG are 72 and 34 cm⁻¹, respectively, consistent with previously reported values.²¹ Finally, in Stage 4, the Raman spectra are compared after annealing at 350 °C for 10 h in a flow of Ar/H₂ (10%) mixture. While Raman spectra show whether layers are fluorinated, they do not show which surfaces of each layer are fluorinated; for that, we must compare how the spectra evolve. It is clear that annealing defluorinates the top surface but not the bottom surface of monolayer graphene on substrates since the atoms on the bottom surface are completely trapped at the interface of graphene and substrate during the annealing process. Thus, comparing the Raman spectra after annealing enables inference of whether the top surface or both top and bottom surfaces are fluorinated. After annealing, the Raman spectrum of the FBG on hBN shows that FBG mostly returns to the original pristine state, with only a small D peak remaining (see more details about uniform and effective removal of F atoms via the annealing process in Figures S6 and S7). Although there is a small D peak remaining as reported, 36 the residual disorder from functionalization is smaller than the underlying hBN peak, suggesting that the vast majority of F atoms have desorbed. Meanwhile, after annealing, the Raman spectrum of the FBG on SiO2 is changed back to the spectrum observed in the FBG on hBN at Stage 3 with a large D peak and distinct 2D peak, indicating that one layer is fluorinated, and the other layer is pristine. Moreover, after annealing the double-sided FBG on SiO2, its fwhm changed to 37 cm⁻¹, very close to the 34 cm⁻¹ fwhm of single-sided FBG on hBN before the annealing (Figure 2c). This indicates that double-sided FBG on SiO₂ is changed to

single-sided FBG after the defluorination of the top F atoms by the annealing.

As an additional confirmation that only the top surface fluorine atoms are desorbed during annealing, we performed the same annealing measurement with fluorinated monolayer graphene on both SiO₂ and hBN, leading to double- and single-sided fluorinated monolayer graphene, respectively (Figure S8). After annealing, the double-sided fluorinated monolayer graphene maintained a large D peak and suppressed 2D peak; meanwhile, the single-sided fluorinated monolayer graphene returned to a pristine state.

Taking the Raman spectra at each stage into account, Figure 2c,d diagrammatically shows the evolution of the bilayer graphene structure through the fluorination stages on SiO2 and hBN substrates, respectively. In Stage 1, both bilayers are in a pristine state. In Stage 2, under initial fluorination, the top surface of the upper layer of both bilayers become functionalized. In Stage 3, both the top and bottom surfaces of the bilayer graphene on SiO2 become fluorinated while only the top surface of the bilayer graphene on hBN becomes fluorinated, effectively decoupling the underlying pristine bottom layer. In Stage 4, after annealing, the fluorine atoms on the top surface of the bilayer graphene on SiO2 are removed, but the trapped fluorine atoms on the bottom layer are maintained. Meanwhile, the fluorine atoms on the top surface of the bilayer graphene on hBN are removed, leaving pristine bilayer graphene.

The different behavior observed for the bilayer graphene on the two substrates is a result of differences in the substrate interaction with the graphene. Since the surface of SiO2 is rough compared to atomically smooth hBN, 37 small gaps form due to nonconformal contact between graphene and SiO₂. The XeF₂ gas permeates through these gaps to fluorinate the bottom surface of the bottom layer. Thus, both the top surface of the upper layer and the bottom surface of the lower layer of bilayer graphene on SiO₂ will be fluorinated, leading to doublesided FBG on SiO₂. In contrast, XeF₂ gas cannot permeate through the gap of the graphene-hBN interface, as the interlayer distance between graphene and hBN is as small as that of graphite. 37-39 As a result, only the top surface of bilayer graphene on hBN is fluorinated, and the bottom layer is left intact, leading to single-sided FBG on hBN. This observation is consistent with multiple studies showing that gas and residue may be trapped in bubbles in 2D heterostructures due to the good seal between layers.⁴⁰

The result reported here on the double-sided FBG is inconsistent with one report that only the top surface of bilayer graphene will be functionalized on SiO₂ by oxygen plasma.²¹ This discrepancy is explained by a difference in processing conditions and demonstrates another way to tune the structure. When annealing graphene, a process commonly used to remove processing residue, the graphene will relax into the nanoscale features, 41 leading to liquidlike adhesion instead of the semisuspended structures. 42 To verify this hypothesis and explain the discrepancy, we annealed the bilayer graphene exfoliated on SiO₂ at 350 °C for 10 h in a flow of Ar/H₂ (10%) mixture, before the initial exposure to XeF2 gas. Figure 3a shows the Raman spectra of the preannealed bilayer graphene on SiO₂ before and after exposure to XeF₂ for 21 min. The postfluorinated Raman spectra of the annealed bilayer graphene on SiO2 show the combination of both sharp and broad 2D peaks rather than the only broad 2D peak observed in the unannealed bilayer graphene on SiO₂ shown in Stage 3

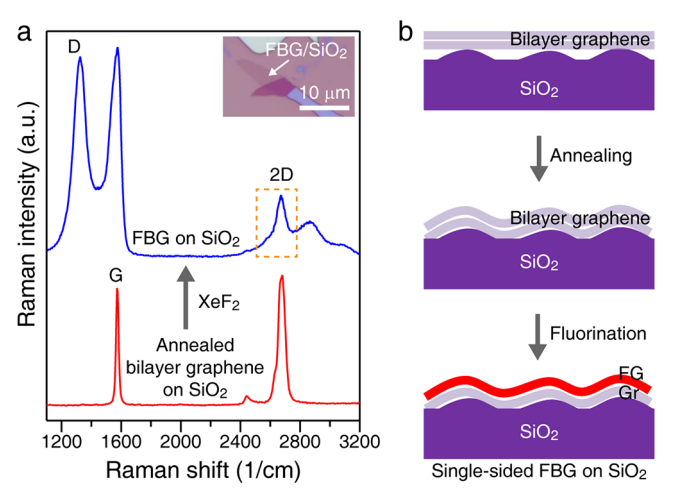


Figure 3. Fluorination of the annealed bilayer graphene on SiO₂. (a) Change in Raman signal of the annealed bilayer graphene on SiO₂ after fluorination for 21 min. The inset is an optical image of annealed bilayer graphene on the SiO₂ surface after fluorination. (b) Schematic illustration presenting the fluorination process of the annealing bilayer graphene on SiO₂. After annealing, as-exfoliated bilayer graphene on the uneven SiO₂ surface forms the conformable structure following the roughness of SiO₂; thereby, only the top graphene layer is changed to fluorinated graphene because the conformable interface between bilayer graphene and SiO₂ prevents the penetration of XeF₂ gas.

of Figures 2a, indicating that the preannealed bilayer graphene turned to single-sided FBG, in agreement with the previous study reporting the single-sided oxidation of preannealed bilayer graphene on $\mathrm{SiO_2}$. Figure 3b shows the evolution in the structure of the annealed bilayer graphene. Conformal contact between graphene and $\mathrm{SiO_2}$ was achieved by annealing, leading to shrinkage of the graphene— $\mathrm{SiO_2}$ interface gap. Since $\mathrm{XeF_2}$ gas cannot permeate through this reduced gap, only the top surface of bilayer graphene is fluorinated as observed in single-sided FBG on hBN substrate. This result confirms that interaction of graphene with the substrate is a critical factor to determine the single- or double-sided fluorination of graphene and shows that impermeable contact between the graphene and substrate can be achieved by using ultraflat substrates or by annealing.

Finally, we compare the electrical properties of the doublesided and single-sided FBGs by measuring the evolution in the gate-dependent resistivity of the bilayer graphene FET (the same device depicted in Figures 1 and 2) under fluorination. As shown in Figure 4a, the pristine bilayer graphene on a SiO₂ substrate, corresponding to Stage 1, had a low resistivity of <1 $k\Omega~\mu m$ over the entire gate voltage range. As is common for graphene on SiO₂ substrates, it was heavily p-doped.⁴³ Under fluorination, the bilayer graphene becomes double-side fluorinated (Stage 2) as shown in Figure 2a,c. Correspondingly, resistivity increased with fluorination time, rising to >2 $G\Omega$ μ m with no gate tunability after 21 min of fluorination (Stage 3). This result is consistent with previous reports of single-sided and double-sided fluorinated monolayer graphene becoming totally insulating.³³ As shown in Figure 4b, the pristine bilayer graphene on the hBN substrate (Stage 1) showed a lower resistivity and charge neutrality point (CNP) around zero gate voltage due to less charged impurities of hBN and ultraclean heterointerfaces of graphene and hBN.³⁷ Under fluorination, the bilayer graphene becomes single-side

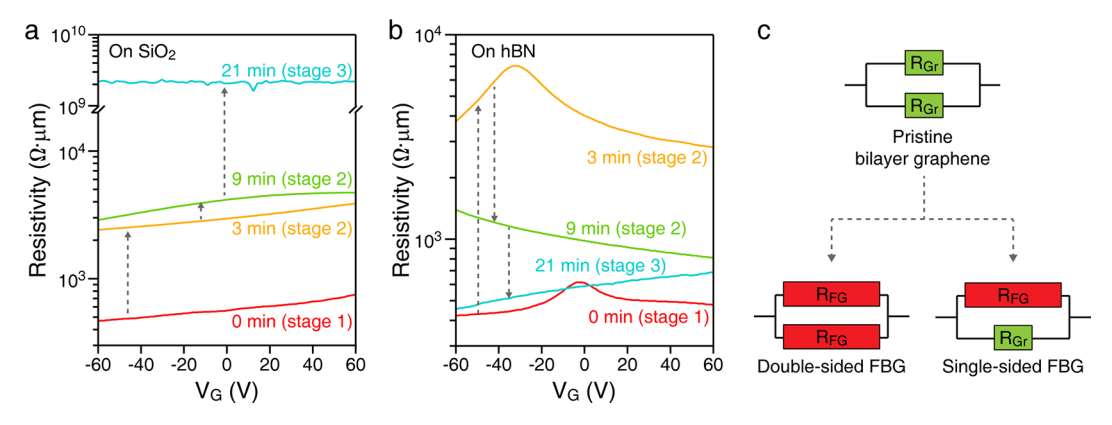


Figure 4. Electrical properties of bilayer graphene devices via the fluorination. Resistivity of (a) bilayer graphene on SiO₂ and (b) bilayer graphene on hBN versus the back-gate bias with 10 mV of the drain-source bias ($V_{\rm ds}$) as fluorination time increases. (c) Schematic representation illustrating the two-channel model. The resistance of conducting graphene (Gr) and insulating fluorinated graphene (FG) is denoted as $R_{\rm Gr}$ and $R_{\rm FG}$, respectively.

fluorinated, as shown in Figure 2b,d. After fluorination of bilayer graphene on hBN for 3 min (in Stage 2), the top surface of bilayer graphene is partially fluorinated, but the two graphene layers are still electrically coupled, where the electronic states are distributed through both in both layers. The partial fluorination leads to electrical disorder and charge localization, where conductivity is dominated by hopping and percolation of the electrons rather than scattering.⁴⁴ Interestingly, under increased fluorination time, the resistivity started to decrease. After 21 min (Stage 3), the single-sided FBG on hBN showed a resistivity as low as that of the pristine bilayer graphene, corresponding with a field-effect mobility of 600 cm² V^{-1} s⁻¹, but with a highly positive CNP. In the contacts of single-sided FBG device shown in Figure 4b, the current flows from the metal electrode to the bottom graphene by tunneling through the top insulating FG (see Figure S9),45 and the measured contact resistance of the single-sided FBG device is about 250–350 Ω μ m at $n = -2 \times 10^{12}$ cm⁻² (see Figure S9). Although the top FG in single-sided FBG is insulating, the results indicate that the bottom graphene layer under the fluorinated top layer still is functioning as a conducting channel, and FG is used as a tunnel contact.2

In Figure 4c, we explain the changes in electrical resistivity of the single-sided and double-sided FBG in the context of the fluorination models of Figure 2c,d. Initially, bilayer graphene can be thought of as two channels connected through a large vertical resistance. For double-sided FBG, both channels become insulating due to the simultaneous fluorination. For single-sided FBG, the fluorinated top layer becomes insulating; meanwhile, the intact bottom layer maintains its conductive channel. Moreover, although the top insulating FG and the bottom conducting graphene are electrically decoupled, the mobility of the bottom graphene under the top FG is lower than that of isolated pristine monolayer graphene, probably due to interlayer carrier scattering by the electric dipole of the top FG. 20,46

CONCLUSIONS

In conclusion, we demonstrate the synthesis of single-sided and double-sided FBG and characterized their structural and electrical properties. Our results show that substrate interactions determine whether bilayer graphene will be single-sided or double-sided functionalized, and these interactions may be tailored. The different functionalization

structures display a distinct electronic behavior. Double-sided functionalized bilayer graphene is fully insulating. In contrast, in single-sided functionalized, the layers effectively decouple, with one layer insulating and the other conducting. Our work provides a new strategy to fabricate other new synthetic 2D materials and graphene-based heterostructures with non-symmetric chemical bonds by using subtle differences in processing that are applicable to electronic, spintronic, and biomedical devices.

METHODS

Fabrication of Bilayer Graphene Samples. We use the silicon (Si) substrate (Nova Electronic Materials) with 285 nm thick thermally grown silicon dioxide (SiO₂) over a Si wafer with no surface treatments, and the surface roughness of SiO₂ is about 0.5 nm. To fabricate the bilayer graphene samples, we use established 2D material pickup techniques.^{24,25*} Before creating the heterostructure, it is necessary to fabricate a sacrificial transfer substrate. First, a 0.5 mm thick polydimethylsiloxane (PDMS) droplet is deposited on a microscope glass slide; then, it was cured overnight at 60 °C. At the same time, poly(bisphenol A carbonate) (Sigma-Aldrich) (PC) dissolved in chloroform was deposited onto a microscope slide glass. The chloroform was evaporated in air at room temperature, and then, the remaining PC film was manually delaminated. The PC film was then placed onto the PDMS, and the entire structure was baked at 170 °C for 15 min to form conformal contact between PC film and PDMS. The resulting transfer substrate was then fixed to a micromanipulator. In parallel, all 2D flakes used for the van der Waals (vdW) heterostructures were separately exfoliated onto the SiO₂ (285 nm)/Si substrates with the scotch tape method. The thickness or layer number of each material is separately confirmed using a combination of Raman spectroscopy, atomic force microscopy, and optical microscopy. For the first pickup, it is necessary to start with an extra thick layer of hBN (~20 nm). The PC/PDMS stamp was placed onto the target hBN flake at 80 °C. To increase adhesion strength between PC and hBN, the temperature was then raised to 130 °C. Then, the PC/PDMS stamp was gradually lifted up during cooling to 80 °C. This process was then repeated to pick up other 2D flakes. After stacking, the whole stacked heterostructure was transferred onto a clean SiO₂/Si substrate by releasing the PC film from the PDMS at a higher temperature of around 175 °C.

Lastly, the PC film was removed by rinsing the sample in chloroform.

Etching of hBN and Fluorination of Bilayer Graphene via XeF₂ **Gas.** The XeF₂ etcher (Xactix etching system) was used for both the etching of top hBN and the fluorination of the bilayer graphene in pulse mode with $P_{\text{XeF}_2} = 3$ Torr at room temperature. We controlled the pulse time, i.e., the exposure time, to change the degree of both the etching and the fluorination.

Raman Spectroscopy. Raman signals were acquired on a Renishaw instrument using a 532 nm laser and 600 l/mm grating. To minimize damage of graphene by irradiation of the laser, a power of <5 mW was used with an acquisition of 60 s.

Transmission Electron Microscopy. TEM images and selected area electron diffraction were acquired using a double Cs-corrected JEOL ARM-200F instrument operated at 80 kV.

Defluorination via Annealing. The fluorinated bilayer graphene (FBG) was defluorinated by the annealing at 350 $^{\circ}$ C for 10 h under the Ar/H₂ (10%) forming gas at atmospheric pressure.

ASSOCIATED CONTENT

3 Supporting Information

The Supporting Information is available free of charge at https://pubs.acs.org/doi/10.1021/acs.nanolett.0c03237.

Additional figures showing the schematic illustration on the fabrication process, AFM of the device, TEM data of samples, and the Raman signals of bilayer graphene via fluorination (PDF)

AUTHOR INFORMATION

Corresponding Authors

Arend M. van der Zande – Department of Mechanical Science and Engineering, University of Illinois Urbana—Champaign, Urbana, Illinois 61801, United States; orcid.org/0000-0001-5104-9646; Email: arendv@illinois.edu

Gwan-Hyoung Lee — Department of Materials Science and Engineering, Research Institute of Advanced Materials (RIAM), Institute of Engineering Research, and Institute of Applied Physics, Seoul National University, Seoul 08826, Korea; orcid.org/0000-0002-3028-867X; Email: gwanlee@snu.ac.kr

Authors

Jangyup Son — Department of Materials Science and Engineering, Seoul National University, Seoul 08826, Korea; Department of Mechanical Science and Engineering, University of Illinois Urbana—Champaign, Urbana, Illinois 61801, United States; Functional Composite Materials Research Center, Korea Institute of Science and Technology (KIST), Jeonbuk 55324, Korea

Huije Ryu – Department of Materials Science and Engineering, Seoul National University, Seoul 08826, Korea

Junyoung Kwon – Department of Materials Science and Engineering, Yonsei University, Seoul 03722, Korea

Siyuan Huang – Department of Mechanical Science and Engineering, University of Illinois Urbana—Champaign, Urbana, Illinois 61801, United States

Jaehyung Yu — Department of Mechanical Science and Engineering, University of Illinois Urbana—Champaign, Urbana, Illinois 61801, United States; orcid.org/0000-0002-9925-2309

Jingwei Xu — Department of Mechanical Science and Engineering, University of Illinois Urbana—Champaign, Urbana, Illinois 61801, United States

Kenji Watanabe — Research Center for Functional Materials, National Institute for Materials Science (NIMS), Ibaraki 305-0044, Japan; orcid.org/0000-0003-3701-8119

Takashi Taniguchi — International Center for Materials Nanoarchitectonics, National Institute for Materials Science (NIMS), Ibaraki 305-0044, Japan; orcid.org/0000-0002-1467-3105

Eunji Ji — Department of Materials Science and Engineering, Yonsei University, Seoul 03722, Korea

Sol Lee – Department of Physics, Yonsei University, Seoul 03722, Korea

Yongjun Shin — Department of Materials Science and Engineering, Seoul National University, Seoul 08826, Korea Jong Hun Kim — Department of Materials Science and Engineering, Seoul National University, Seoul 08826, Korea Kwanpyo Kim — Department of Physics, Yonsei University, Seoul 03722, Korea; orcid.org/0000-0001-8497-2330

Complete contact information is available at: https://pubs.acs.org/10.1021/acs.nanolett.0c03237

Author Contributions

J.S., A.M.v.d.Z., and G.-H.L. conceived and designed the study. J.S. fabricated samples and carried out experiments under the guidance of A.M.v.d.Z. and G.-H.L. with the help of the other authors. H.R. and J.K. fabricated the bilayer graphene devices. S.H. helped to carry out the AFM experiment. J.Y. and J.X. provided graphene and helped the defluorination via the annealing. K.W. and T.T. prepared high-quality hBN. E.J. prepared CVD graphene samples for TEM analysis. S.L. and K.K. helped to carry out the TEM experiment. Y.S. and J.K. helped to carry out the PES experiment. All authors contributed to the discussion of this work. J.S., A.M.v.d.Z., and G.-H.L. wrote the manuscript with the help of the other authors.

Notes

The authors declare no competing financial interest.

ACKNOWLEDGMENTS

This work was supported by National Research Foundation (NRF) funded by the Ministry of Science, ICT & Future Planning by the Korean government (2018M3D1A1058793, 2017R1A5A1014862, SRC program: vdWMRC center), the New Faculty Startup Fund and Creative-Pioneering Researchers Program from Seoul National University. A.M.v.d.Z. acknowledges support from NSF-MRSEC under Award Number DMR-1720633, the NSF-CAREER award under Award Number CMMI-1846732, and TSMC Grant under Award Number TSMC Taiwan 089401. J.S. acknowledges support from the KIST Institution Program (2K02420, 2Z06030). K.W. and T.T. acknowledge support from the Elemental Strategy Initiative conducted by the MEXT, Japan, Grant Number JPMXP0112101001, JSPS KAKENHI Grant Numbers JP20H00354 and the CREST(JPMJCR15F3), JST. K.K. acknowledges support from Basic Science Research Program through the National Research Foundation of Korea (NRF-2017R1A5A1014862).

REFERENCES

- (1) Li, L.; Lu, S.-Z.; Pan, J.; Qin, Z.; Wang, Y.-Q.; Wang, Y.; Cao, G.-Y.; Du, S.; Gao, H.-J. Buckled Germanene Formation on Pt (111). *Adv. Mater.* **2014**, *26*, 4820–4824.
- (2) Mannix, A. J.; Zhou, X.-F.; Kiraly, B.; Wood, J. D.; Alducin, D.; Myers, B. D.; Liu, X.; Fisher, B. L.; Santiago, U.; Guest, J. R.; Yacaman, M. J.; Ponce, A.; Oganov, A. R.; Hersam, M. C.; Guisinger, N. P. Synthesis of Borophenes: Anisotropic, Two-dimensional Boron Polymorphs. *Science* 2015, 350, 1513–1516.
- (3) Zhao, J.; Liu, H.; Yu, Z.; Quhe, R.; Zhou, S.; Wang, Y.; Liu, C. C.; Zhong, H.; Han, N.; Lu, J.; Yao, Y.; Wu, K. Rise of Silicene: A Competitive 2D Material. *Prog. Mater. Sci.* **2016**, 83, 24–151.
- (4) Lu, A.-Y.; Zhu, H.; Xiao, J.; Chuu, C.-P.; Han, Y.; Chiu, M.-H.; Cheng, C.-C.; Yang, C.-W.; Wei, K.-H.; Yang, Y.; Wang, Y.; Sokaras, D.; Nordlund, D.; Yang, P.; Muller, D. A.; Chou, M.-Y.; Zhang, X.; Li, L.-J. Janus Monolayers of Transition Metal Dichalcogenides. *Nat. Nanotechnol.* **2017**, *12*, 744–749.
- (5) Ong, M. T.; Duerloo, K.-A. N.; Reed, E. J. The Effect of Hydrogen and Fluorine Coadsorption on the Piezoelectric Properties of Graphene. *J. Phys. Chem. C* **2013**, *117*, 3615–3620.
- (6) Bakharev, P. V.; Huang, M.; Saxena, M.; Lee, S. W.; Joo, S. H.; Park, S. O.; Dong, J.; Camacho-Mojica, D.; Jin, S.; Kwon, Y.; Biswal, M.; Ding, F.; Kwak, S. K.; Lee, Z.; Ruoff, R. S. Chemically Induced Transformation of Chemical Vapor Deposition Grown Bilayer Graphene into Fluorinated Single-Layer Diamond. *Nat. Nanotechnol.* **2020**, *15*, 59–66.
- (7) Son, J.; Buzov, N.; Chen, S.; Sung, D.; Ryu, H.; Kwon, J.; Kim, S.; Namiki, S.; Hong, S.; Watanabe, K.; Taniguchi, T.; King, W. P.; Lee, G.-H.; van der Zande, A. M. Tailoring Surface Properties via Functionalized Hydrofluorinated Graphene Compounds. *Adv. Mater.* **2019**, *31*, 1903424.
- (8) Craciun, M. F.; Khrapach, I.; Barnes, M. D.; Russo, S. Properties and Applications of Chemically Functionalized Graphene. *J. Phys.: Condens. Matter* **2013**, *25*, 423201.
- (9) Novoselov, K. S.; Geim, A. K.; Morozov, S. V.; Jiang, D.; Zhang, Y.; Dubonos, S. V.; Grigorieva, I. V.; Firsov, A. A. Electric Field Effect in Atomically Thin Carbon Films. *Science* **2004**, *306*, 666–669.
- (10) Geim, A. K.; Novoselov, K. S. The Rise of Graphene. *Nat. Mater.* **2007**, *6*, 183–191.
- (11) Bolotin, K. I.; Sikes, K. J.; Kilma, M.; Fudenberg, G.; Hone, J.; Kim, P.; Stormer, H. L. Ultrahigh Electron Mobility in Suspended Graphene. *Solid State Commun.* **2008**, *146*, 351–355.
- (12) Castro Neto, A. H.; Guinea, F.; Peres, N. M. R.; Novoselov, K. S.; Geim, A. K. The Electronic Properties of Graphene. *Rev. Mod. Phys.* **2009**, *81*, 109–162.
- (13) Yu, Y.-J.; Zhao, Y.; Ryu, S.; Brus, L. E.; Kim, K. S.; Kim, P. Tuning the Graphene Work Function by Electric Field Effect. *Nano Lett.* **2009**, *10*, 3430–3434.
- (14) Allen, M. J.; Tung, V. C.; Kaner, R. B. Honeycomb Carbon: A Review of Graphene. *Chem. Rev.* **2010**, *110*, 132–145.
- (15) Craciun, M. F.; Russo, S.; Yamamoto, M.; Tarucha, S. Tuneable Electronic Properties in Graphene. *Nano Today* **2011**, *6*, 42–60.
- (16) Kim, S. J.; Choi, K.; Lee, B.; Kim, Y.; Hong, B. H. Materials for Flexible, Stretchable Electronics: Graphene and 2D Materials. *Annu. Rev. Mater. Res.* **2015**, 45, 63–84.
- (17) Papageorgiou, D. G.; Kinloch, I. A.; Young, R. J. Mechanical Properties of Graphene and Graphene-Based Nanocomposites. *Prog. Mater. Sci.* **2017**, *90*, 75–127.
- (18) Dreyer, D. R.; Park, S.; Bielawski, C. W.; Ruoff, R. S. The Chemistry of Graphene Oxide. *Chem. Soc. Rev.* **2010**, *39*, 228–240.
- (19) Pumera, M.; Wong, C. H. A. Graphene and Hydrogenated Graphene. Chem. Soc. Rev. 2013, 42, 5987–5995.
- (20) Feng, W.; Long, P.; Feng, Y.; Li, Y. Two-Dimensional Fluorinated Graphene: Synthesis, Structures, Properties and Applications. *Adv. Sci.* **2016**, *3*, 1500413.
- (21) Felten, A.; Flavel, B. S.; Britnell, L.; Eckmann, A.; Louette, P.; Pireaux, J.-J.; Hirtz, M.; Krupke, R.; Casiraghi, C. Single- and Double-Sided Chemical Functionalization of Bilayer Graphene. *Small* **2013**, *9*, 631–639.

- (22) Santos, H.; Henrard, L. Fluorine Adsorption on Single and Bilayer Graphene: Role of Sublattice and Layer Decoupling. *J. Phys. Chem. C* 2014, *118*, 27074–27080.
- (23) Fang, W.; Hsu, A. L.; Caudillo, R.; Song, Y.; Birdwell, A. G.; Zakar, E.; Kalbac, M.; Dubey, M.; Palacios, T.; Dresselhaus, M. S.; Araujo, P. T.; Kong, J. Rapid Identification of Stacking Orientation in Isotopically Labeled Chemical-Vapor Grown Bilayer Graphene by Raman Spectroscopy. *Nano Lett.* 2013, 13, 1541–1548.
- (24) Weis, J. E.; Costa, S. D.; Frank, O.; Bastl, Z.; Kalbac, M. Fluorination of Isotopically Labeled Turbostratic and Bernal Stacked Bilayer Graphene. *Chem. Eur. J.* **2015**, *21*, 1081–1087.
- (25) Georgakilas, V.; Otyepka, M.; Bourlinos, A. B.; Chandra, V.; Kim, N.; Kemp, K. C.; Hobza, P.; Zboril, R.; Kim, K. S. Functionalization of Graphene: Covalent and Non-Covalent Approaches, Derivatives and Applications. *Chem. Rev.* **2012**, *112*, 6156–6214.
- (26) Wang, L.; Meric, I.; Huang, P. Y.; Gao, Q.; Gao, Y.; Tran, H.; Taniguchi, T.; Watanabe, K.; Campos, L. M.; Muller, D. A.; Guo, J.; Kim, P.; Hone, J.; Shepard, K. L.; Dean, C. R. One-Dimensional Electrical Contact to A Two-Dimensional Material. *Science* **2013**, *342*, 614–617
- (27) Pizzocchero, F.; Gammelgaard, L.; Jessen, B. S.; Caridad, J. M.; Wang, L.; Hone, J.; Bøggild, P.; Booth, T. J. The Hot Pick-Up Technique for Batch Assembly of van der Waals Heterostructures. *Nat. Commun.* **2016**, *7*, 11894.
- (28) Son, J.; Kwon, J.; Kim, S.; Lv, Y.; Yu, J.; Lee, J.-Y.; Ryu, H.; Watanabe, K.; Taniguchi, T.; Garrido-Menacho, R.; Mason, N.; Ertekin, E.; Huang, P. Y.; Lee, G.-H.; van der Zande, A. M. Atomically Precise Graphene Etch Stops for Three Dimensional Integrated Systems from Two Dimensional Material Heterostructures. *Nat. Commun.* **2018**, *9*, 3988.
- (29) Bunch, J. S.; Verbridge, S. S.; Alden, J. S.; van der Zande, A. M.; Parpia, J. M.; Craighead, H. G.; McEuen, P. L. Impermeable Atomic Membranes from Graphene Sheets. *Nano Lett.* **2008**, *8*, 2458–2462.
- (30) Ferrari, A. C.; Meyer, J. C.; Scardaci, V.; Casiraghi, C.; Lazzeri, M.; Mauri, F.; Piscanec, S.; Jiang, D.; Novoselov, K. S.; Roth, S.; Geim, A. K. Raman Spectrum of Graphene and Graphene Layers. *Phys. Rev. Lett.* **2006**, *97*, 187401.
- (31) Garcia, A. G. F.; Neumann, M.; Amet, F.; Williams, J. R.; Watanabe, K.; Taniguchi, T.; Goldhaber-Gordon, D. Effective Cleaning of Hexagonal Boron Nitride for Graphene Devices. *Nano Lett.* **2012**, *12*, 4449–4454.
- (32) Nair, R. R.; Ren, W.; Jalil, R.; Riaz, I.; Kravets, V. G.; Britnell, L.; Blake, P.; Schedin, F.; Mayorov, A. S.; Yuan, S.; Katsnelson, M. I.; Cheng, H.-M.; Strupinski, W.; Bulusheva, L. G.; Okotrub, A. V.; Grigorieva, I. V.; Grigorenko, A. N.; Novoselov, K. S.; Geim, A. K. Fluorographene: A Two-Dimensional Counterpart of Teflon. *Small* **2010**, *6*, 2877–2884.
- (33) Robinson, J. T.; Burgess, J. S.; Junkermeier, C. E.; Badescu, S. C.; Reinecke, T. L.; Perkins, F. K.; Zalalutdniov, M. K.; Baldwin, J. W.; Culbertson, J. C.; Sheehan, P. E.; Snow, E. S. Properties of Fluorinated Graphene Films. *Nano Lett.* **2010**, *10*, 3001–3005.
- (34) Stine, R.; Lee, W. K. E., Jr; Robinson, J. T.; Sheehan, P. E. Chemical Stability of Graphene Fluoride Produced by Exposure to XeF₂. *Nano Lett.* **2013**, *13*, 4311–4316.
- (35) Kashtiban, R. J.; Dyson, M. A.; Nair, R. R.; Zan, R.; Wong, S. L.; Ramasse, Q.; Geim, A. K.; Bangert, U.; Sloan, J. Atomically Resolved Imaging of Highly Ordered Alternating Fluorinated Graphene. *Nat. Commun.* **2014**, *5*, 4902.
- (36) Costa, S. D.; Weis, J. E.; Frank, O.; Bastl, Z.; Kalbac, M. Thermal Treatment of Fluorinated Graphene: An in situ Raman Spectroscopy Study. *Carbon* **2015**, *84*, 347–354.
- (37) Dean, C. R.; Young, A. F.; Meric, I.; Lee, C.; Wang, L.; Sorgenfrei, S.; Watanabe, K.; Taniguchi, T.; Kim, P.; Shepard, K. L.; Hone, J. Boron Nitride Substrates for High-Quality Graphene Electronics. *Nat. Nanotechnol.* **2010**, *5*, 722–726.
- (38) Haigh, S. J.; Gholinia, A.; Jalil, R.; Romani, S.; Britnell, L.; Elias, D. C.; Novoselov, K. S.; Ponomarenko, L. A.; Geim, A. K.; Gorbachev, R. Cross-Sectional Imaging of Individual Layers and

- Buried Interfaces of Graphene-based Heterostructures and Superlattices. *Nat. Mater.* **2012**, *11*, 764–767.
- (39) Gopinadhan, K.; Hu, S.; Esfandiar, A.; Lozada-Hidalgo, M.; Wang, F. C.; Yang, Q.; Tyurnina, A. V.; Keerthi, A.; Radha, B.; Geim, A. K. Complete Steric Exclusion of Ions and Proton Transport through Confined Monolayer Water. *Science* **2019**, 363, 145–148.
- (40) Khestanova, E.; Guinea, F.; Fumagalli, L.; Geim, A. K.; Grigorieva, I. V. Universal Shape and Pressure Inside Bubbles Appearing in van der Waals Heterostructures. *Nat. Commun.* **2016**, *7*, 12587.
- (41) Yu, Y.-J.; Lee, G.-H.; Choi, J. I.; Shim, Y. S.; Lee, C.-H.; Kang, S. J.; Lee, S.; Rim, K. T.; Flynn, G. W.; Hone, J.; Kim, Y.-H.; Kim, P.; Nuckolls, C.; Ahn, S. Epitaxially Self-Assembled Alkane Layers for Graphene Electronics. *Adv. Mater.* **2017**, *29*, 1603925.
- (42) Das, S.; Lahiri, D.; Agarwal, A.; Choi, W. Interfacial Bonding Characteristics between Graphene and Dielectric Substrates. *Nanotechnology* **2014**, *25*, 045707.
- (43) Ryu, S.; Berciaud, S.; Yu, Y.-J.; Liu, H.; Kim, P.; Flynn, G. W.; Brus, L. E. Atmospheric Oxygen Binding and Hole Doping in Deformed Graphene on a SiO₂ Substrate. *Nano Lett.* **2010**, *10*, 4944–4951
- (44) Stabile, A. A.; Ferreira, A.; Li, J.; Peres, N. M. R.; Zhu, J. Electrically tunable resonant scattering in fluorinated bilayer graphene. *Phys. Rev. B: Condens. Matter Mater. Phys.* **2015**, 92, No. 121411(R).
- (45) Cui, X.; Shih, E.-M.; Jauregui, L. A.; Chae, S. H.; Kim, Y. D.; Li, B.; Seo, D.; Pistunova, K.; Yin, J.; Park, J.-H.; Choi, H.-J.; Lee, Y. H.; Watanabe, K.; Taniguchi, T.; Kim, P.; Dean, C. R.; Hone, J. C. Low-Temperature Ohmic Contact to Monolayer MoS₂ by van der Waals Bonded Co/h-BN Electrodes. *Nano Lett.* **2017**, *17*, 4781–4786.
- (46) Wang, Y.; Lee, W. C.; Manga, K. K.; Ang, P. K.; Lu, J.; Liu, Y. P.; Lim, C. T.; Loh, K. P. Fluorinated Graphene for Promoting Neuro-Induction of Stem Cells. *Adv. Mater.* **2012**, *24*, 4285–4290.